Engineered synthetic scaffolds for organizing proteins within the bacterial cytoplasm

Authors: Matthew J. Lee,[1] Judith Mantell,[2,3] Lorna Hodgson,[2] Dominic Alibhai,[2] Jordan M Fletcher,[4] Ian R. Brown,[1] Stefanie Frank,[5] Wei-Feng Xue,[1] Paul Verkade,[2,3,6] Derek N Woolfson,[2,4,6]* Martin J Warren[1]*.

[1]Industrial Biotechnology Centre, School of Biosciences, University of Kent, Canterbury CT2 7NJ, UK

[2]School of Biochemistry, University of Bristol, Medical Sciences Building, University Walk, Bristol BS8 1TD, UK.

[3]Wolfson Bioimaging Facility, Medical Sciences Building, University Walk, Bristol BS8 1TD, UK.

[4]School of Chemistry, University of Bristol, Cantock's Close, Bristol BS8 1TS, UK.

[5]Department of Biochemical Engineering, University College London, Bernard Katz Building, Gordon Street, London WC1E 6BT, UK.

[6]BrisSynBio, Life Sciences Building, Tyndall Avenue, Bristol BS8 1TQ, UK.

* Correspondence to: Martin J Warren (M.J. Warren@kent.ac.uk) and Derek N Woolfson (D.N.Woolfson@bristol.ac.uk)

Abstract:

We have developed a system for producing a supramolecular scaffold that permeates the entire *Escherichia coli* cytoplasm. This cytoscaffold is constructed from a three-component system comprising a bacterial microcompartment shell protein and two complementary *de novo* coiled-coil peptides. We show that other proteins can be targeted to this intracellular filamentous arrangement. Specifically, the enzymes pyruvate decarboxylase and alcohol dehydrogenase have been directed to the filaments, leading to enhanced ethanol production in these engineered bacterial cells compared with those that do not produce the scaffold. This is consistent with improved metabolic efficiency through enzyme colocation. Finally, the shell-protein scaffold can be directed to the inner membrane of the cell, demonstrating how synthetic cellular organization can be coupled with spatial optimization through in-cell protein design. The cytoscaffold has potential for the development of next-generation cell factories, where it could be used to organize enzyme pathways and metabolite transporters to enhance metabolic flux.

Introduction:

In industrial biotechnology and synthetic biology there is a growing need to generate internal bacterial supramolecular scaffolds *en route* to delivering so-called cell factories[1]. To this end, researchers have investigated protein-based linkers[2], lipids[3] and nucleic acids[4,5] as modulators to attain high-level biomolecular organization. However, none of these approaches have delivered a uniform matrix throughout a bacterial cytoplasm. The advantage of such scaffolding systems is that they can be used to direct and align biosynthetic pathway enzymes to orchestrate greater production of commodity and speciality chemicals, especially in pathways that proceed through unstable or toxic intermediates[6,7]. This is because the close proximity of enzymes on a scaffold allow for greater channeling of intermediates through improved flux, stabilization of intermediates and protection from other reactions[8,9].

A number of natural scaffolds are found in bacterial cells. For instance, bacterial microcompartments (BMCs) are organelles with an outer semi-permeable scaffold in the form of a protein shell, which encases a specific metabolic pathway[10-12]. BMCs have a diameter of approximately 150 nm and possess high concentrations of internalized enzymes. This is most apparent in carboxysomes, which are anabolic BMCs where the high concentrations of carbonic anhydrase and RuBisCO ensure enhanced carbon fixation[13,14]. In catabolic BMCs, such as the metabolosome associated with propanediol utilization (the so-called Pdu system), internalized enzymes necessitate that propionaldehyde is rapidly transformed into either an alcohol or a CoA thioester, thereby protecting the cell from the potentially toxic aldehyde intermediate[15-17]. In all cases, the enzymes are targeted to the interior of the BMCs by small encapsulation peptides, which interact with a component of the outer shell scaffold[18-21]. Modelling studies indicate that BMCs enhance flux through intermediate sequestration[22]. Recently, a detailed structure of a recombinant BMC shell has been reported, showing the precise orientation of the different shell proteins that tile together

to form the outer casing, providing molecular detail on how the shell proteins scaffold together to act as a semi-permeable membrane[23].

Apart from BMCs, the other major scaffold within prokaryotic cells is the cytoskeleton[24], which is generally distributed around the inner membrane. This filamentous structure, which includes protein components such as FtsZ, MreB, ParM and MinD[25,26], has roles in cell division, cell morphology and structural polarity. However, the essential nature of these proteins precludes them from being developed as major cellular matrices. For these reasons, we sought to construct a simple and modular bacterial cytoskeleton, which we call a cytoscaffold, from components that we understand and can manipulate predictably.

Previously, we showed that a single shell protein from the *Citrobacter freundii* propanediol utlisation (Pdu) BMC, with a minor modification to its *C* terminus to improve solubility (PduA*), forms filaments in *E. coli*[27]. PduA itself hexamerizes to form a tile that assembles to make the facets of the BMC casing[28,29]. However, when overproduced recombinantly in *E. coli*, PduA* forms hollow filaments approx. 20 nm in diameter that span the length of the cell[30]. Moreover, these structures often interfere with septation during cell division. Nonetheless, we reasoned that PduA*-based filamentous structures could present tractable scaffolds for tethering other proteins.

Here, we describe a three-component system comprising PduA and two complementary *de novo*-designed coiled-coil peptides[31], which form an interactive intracellular filamentous arrangement that gives the appearance of a matrix that permeates the entire *E. coli* cytoplasm (**Supplementary Fig. 1**). We show that other proteins can be specifically targeted to these cytoscaffolds. Building on this, we demonstrate that tethering metabolic enzymes for ethanol production to the PduA scaffold increases their effective local and relative concentrations, and results in improved ethanol production. Finally, we show that the scaffold can be directed to the inner membrane of the cell, further illustrating its modularity,

flexibility, and utility, and demonstrating how synthetic cellular organization can be coupled with spatial optimization.

Results:

Construction of a filamentous scaffold. Initially, we tested if different proteins could be recruited to PduA* filaments *in vivo* in an analogous way to how encapsulation peptides are thought to work in natural BMCs (*vide supra*). Attempts to use the natural encapsulation peptides themselves were not very successful mainly due to aggregation within the cell[32]. Therefore, we turned to a better-characterized *de novo* designed heterodimeric coiled-coil system, CC-Di-AB (ref. 31), which has been used successfully to construct self-assembling peptide cages[33]. The heterodimer comprises two peptides (acidic (A) and basic (B)) that do not self-associate, but do interact specifically and tightly when mixed. The concept was to fuse either CC-Di-A or CC-Di-B to PduA*, and then test if a reporter protein with the cognate peptide could be targeted to the filaments. Plasmids encoding fusion proteins of the following type were made: CC-Di-A/B–Gly/Ser linker–HexaHisTag–PduA*, referred to as CC-Di-A–PduA* and CC-Di-B–PduA*. A control plasmid harboring the fusion without the CC-Di-A/B module, *i.e.* containing only the Gly/Ser linker–HexaHisTag (C–PduA*), was also made. Plasmids were transformed individually into *E. coli* cells and the resulting strains were grown, induced and analyzed by transmission electron microscopy (TEM) after fixation, embedding, thin sectioning and staining.

Strains expressing PduA* alone generated parallel filaments spanning the length of the cell (**Fig. 1a**), and appear to interfere with septation (**Supplementary Fig. 2**). Unexpectedly, the strains producing the control C–PduA* and the CC-Di-A–PduA* did not form any filamentous structures (**Fig. 1b** and **Supplementary Fig. 3**). C–PduA* expression led to deposits of material at the poles of the cell, suggesting that the Gly/Ser linker and/or the hexa-histidine tag alone affects solubility of the fusion protein. This was not seen with CC-Di-A–PduA*, but it is not clear why filaments do not form with this construct. In both cases, western blots revealed only low levels of CC-Di-A–PduA* and C–PduA* fusions in comparison to untagged

PduA*, suggesting potential cytotoxicity of these proteins (**Supplementary Fig. 4**). In contrast, large amounts of CC-Di-B–PduA* were detected in the cells transformed with its plasmid (**Supplementary Fig. 4**), and this led to numerous filaments throughout the cytoplasm (**Fig. 1c** and **Supplementary Fig. 5**). These filaments had a similar 23.6 ± 2.78 nm (n = 100) diameter to untagged PduA* filaments[30], but the former were considerably shorter (**Fig. 1d**,**e**). Consequently, CC-Di-B–PduA* filaments were not aligned within cells, and they did not appear to disrupt cells. It is not clear why the CC-Di-B–PduA* filaments are shortened, but possibly the highly charged CC-Di-B peptide limits filament growth in some way.

Characterization of the cytoscaffold. To probe the spatial localization and organization of the shorter CC-Di-B–PduA* filaments, thicker thin sections (250 nm) were cut and prepared for TEM tomography. Analysis of the resulting tomogram confirmed the presence of the shorter filaments throughout the cytoplasm, except in a central region that is largely occupied by genomic DNA (**Fig. 1f**). Using methods developed to track microtubule assemblies in cells[34], these structures were rendered and visualized in three dimensions (**Fig. 1f** and **Supplementary Videos 1** and **2**). This made clear that the filaments were not aligned but arrayed with multiple orientations, resulting in the appearance of an internal matrix. Analysis of these filaments revealed an average length of 161.2 ± 102.4 nm (n = 739); although, due to the limitation of a 250 nm thin section, the true length is likely longer than this (**Fig. 1e**).

To test the robustness of the CC-Di-B–PduA* filaments, and to interrogate their structure in more detail, the filaments were purified from cells using protocols developed for BMC isolation[21]. Cells were lysed and the filaments were purified by combining centrifugation and differential salt precipitation (**Supplementary Fig. 6**). Purified filaments were analyzed by TEM and AFM. Both confirmed intact filaments, and these approaches provided the opportunity to gain greater insight into the molecular organization of these structures (**Supplementary Fig. 7**). These *ex vivo* filaments tended to cluster together on the TEM

grids and AFM substrates. This clustering was also seen, though to a lesser extent, in some thin sections of whole cells visualized by TEM.

Targeting to and functionalization of the cytoscaffold. Next, we tested if the CC-Di-B peptides of the CC-Di-B–PduA* filaments were available for targeting by other proteins labelled with CC-Di-A using the fluorescent protein citrine. To do this, we made CC-Di-A–citrine and C–Citrine constructs similar in design to the fusion proteins described above. By cloning these constructs in compatible plasmids, they could either be transformed alone or co-transformed with the plasmid producing CC-Di-B–PduA*.

On their own, both CC-Di-A–Citrine and C–Citrine produced uniform fluorescence throughout the cells, consistent with soluble, cytoplasmic proteins (**Supplementary Fig. 8**). Similarly, when co-expressed with CC-Di-B–PduA*, the C–Citrine control produced fluorescence distributed throughout the cell. In contrast, co-expression of CC-Di-A–Citrine and CC-Di-B–PduA* produced more punctate fluorescence, and reduced fluorescence around the genomic DNA (**Fig. 2a**). This is consistent with CC-Di-A–Citrine being localized to the filamentous scaffold. Correlative Light Electron Microscopy (CLEM)[35,36] of high-pressure frozen cells co-expressing CC-Di-A–GFP and CC-Di-B–PduA* confirmed the localization of fluorescence to the intracellular filamentous network (**Fig. 2b**–**e**). Control strains expressing the CC-Di-B–PduA* filaments with untagged GFP showed only a cytoplasmic signal (**Supplementary Fig. 9**). Expression of CC-Di-B–Citrine with or without CC-Di-B–PduA* resulted in punctate fluorescence, suggesting self-association of the CC-Di-B peptide (**Supplementary Fig. 8**).

To demonstrate that multiple cargo proteins could be directed to the cytoscaffold, CC-Di-A–Citrine and a CC-Di-A–mCherry fusion were co-produced in cells with CC-Di-B–PduA* filaments. This gave similar patterns to those observed with CC-Di-A–Citrine plus CC-Di-B–PduA*, and the mCherry and citrine signals co-localized (**Fig. 2f**–**h**).

While the results clearly demonstrate that fluorescent protein can be localized to the PduA* filaments through the use of the coiled-coil interaction, we also wanted to investigate if enzymes could be pegged onto the PduA* filaments in a similar fashion. To investigate this, pyruvate decarboxylase (Pdc) and alcohol dehydrogenase (Adh) were both tagged with the CC-Di-A peptide and co-expressed with and without the CC-Di-B–PduA* filaments. Intriguingly, strains expressing Pdc and Adh grew to a substantially higher OD_{600} in comparison to both control strains (**Supplementary Fig. 10a**). GC/MS analysis of the growth medium revealed that the introduction of the CC-Di-B–PduA* filamentous network increased ethanol production by 221% per OD unit (t = 120 hrs) in comparison to a strain expressing Pdc and Adh but not the cytoscaffold (**Fig. 3** and **Supplementary Fig. 10b**). Western blot analysis showed that this increase in ethanol production was not due to increased protein expression: indeed, the levels of Pdc and Adh were actually reduced by 48 ± 13.3 % and 26 ± 5.5 %, respectively, in the strain expressing CC-Di-A-tagged enzymes in the presence of the CC-Di-B–PduA* filaments (**Supplementary Fig. 11**). The presence of filaments in these strains was confirmed by TEM analysis (**Supplementary Fig. 12**). These experiments provide strong evidence that the localization of enzymes onto the PduA* scaffold substantially enhances an engineered metabolic pathway.

As a final demonstration of the modularity, versatility and potential utility of the new cytoscaffold, we tested if it could be directed to the cytoplasmic side of the inner membrane of *E. coli* (**Fig. 4**). For this, we added the C-terminal membrane-localizing region of MinD from *B. subtilis* to the CC-Di-A–Citrine fusion to render CC-Di-A–Citrine–MinD[37]. When expressed in cells and imaged by confocal fluorescence microscopy, halos around the cytoplasm were evident, indicating localization of the citrine to the cell membrane (**Fig. 4b**). This was also the case for the C–Citrine–MinD control (**Supplementary Fig. 13**). When each of these were co-expressed with CC-Di-B–PduA* filaments, we observed differences in location between control and membrane-targeting constructs (**Fig. 4a**).

First, in cells expressing CC-Di-B–PduA* alone, an average 30% of the filaments were associated with the membrane. For CC-Di-B–PduA* plus the C–Citrine–MinD control this localization was very similar (31%). In contrast, for the CC-Di-B–PduA* plus CC-Di-A–Citrine–MinD combination, 60% of the filaments were localized to the inner membrane, and this difference was statistically significant ($p < 0.01$). One-way ANOVA showed no significant difference ($p < 0.01$) in the total number of filaments between the three strains. Collectively, these analyses demonstrated that the cellular spatial location of the CC-Di-B–PduA* filaments can be controlled by interactions with the cognate *de novo*-designed coiled-coil pair.

Discussion:

Previously, we and others have shown that individual shell proteins, which form the hexameric tiles of the BMC casing, generate long filamentous macromolecular structures when overproduced in the host bacterial cells[30,38]. These structures are particularly apparent with PduA* from the propanediol utlization BMC. The filaments formed by PduA* are approx. 20 nm in diameter. They can be several microns long and have a tendency to stack together and align along the length of the cell, to the extent that they interfere with cell septation. We hypothesized that the PduA* filaments could be formed from the self-association of the hexameric tiles into a protein sheet that then rolls into a nanotubule filament. We wondered if it would be possible to target specific proteins to these filaments to generate higher-order supramolecular organization the cell by design.

To achieve this we have employed a heterodimeric coiled-coil system, CC-Di-A and CC-Di-B (ref. 31), previously characterized and used, for example, in the *de novo* construction of peptide cages[33]. We found that whilst fusion of the CC-Di-A sequence onto PduA* resulted in low protein production and loss of filament formation, the attachment of CC-Di-B to PduA* led to the formation of much shorter filaments that were dispersed throughout the cytoplasm.

227 The reason for the shorter filaments is not clear, but could be due to a slight frustration of
228 hexamer packing when the positively charged CC-Di-B is appended, or from faster
229 nucleation of CC-Di-B–PduA* fusions resulting in a greater number of shorter filaments.
230 Importantly, given the quantity of filaments that are produced throughout the cell, their
231 formation and presence did not appear to alter cell viability or growth.

232 By adding the complementary CC-Di-A peptide onto fluorescent proteins we showed through
233 imaging techniques that these tagged proteins can be recruited to the CC-Di-B–PduA*
234 filaments, demonstrating that the filaments can act as molecular scaffold. A key
235 biotechnological use of scaffolds within a cell would be to localize biosynthetic enzymes in
236 close proximity to one another in order to facilitate metabolic channeling. This is part of the
237 theory behind multi-enzyme complexes, although in these cases, direct transfer or
238 channeling of metabolites from one enzyme to the next also takes place. Using simple
239 systems it has been shown that compartmentalization of pyruvate decarboxylase and
240 alcohol dehydrogenase within a recombinant BMC improves production of ethanol from
241 pyruvate[21]. Similarly, the direct fusion of these two enzymes also results in improved flux[39],
242 indicating, in both cases, that having the second enzyme in close proximity to the first
243 ensures that the unstable acetaldehyde intermediate is more efficiently converted into the
244 alcohol. Therefore, we targeted pyruvate decarboxylase and alcohol dehydrogenase to the
245 PduA filaments using the coiled-coil modules, and much more ethanol was produced in
246 comparison to when the enzymes were expressed in the absence of the scaffold. This
247 provides very strong evidence that the PduA scaffolds can be used to cluster metabolic
248 enzymes in order to accelerate the channeling of intermediates from one enzyme to the
249 next.

250 The CC-Di-B peptide can also be used to control the localization of the PduA filaments
251 within the cell. This was achieved by targeting the CC-Di-A-Citrine protein to the inner
252 membrane by fusing on the MinD membrane-targeting region to the C terminus of the
253 construct. Co-expression of this CC-Di-A–Citrine–MinD protein with CC-Di-B–PduA* directed

filaments to the inner-membrane surface. Such localization strategies could be used to ensure that pathway-enriched filaments have ready access to metabolites that are taken up via transporters, or conversely to ensure that products are generated near the membrane for export out of the cell.

Furthermore, the fact that the CC-Di-B–PduA* filaments are able to interact easily with either cytosolic proteins or membrane-targeted proteins containing the CC-Di-A peptide suggests that the N-terminal region of PduA must be solvent-exposed. The two sides of the hexameric PduA tiles are distinguished by their concave and convex appearance, respectively. The N terminus of PduA, to which CC-Di-B is fused, is located on the concave side of the protein. The fact that this CC-Di-B peptide is available for interaction with a CC-Di-A-tagged protein strongly implies that the filament formed from PduA is generated with the concave side exposed to the solvent. This agrees with the recent structure of a recombinant BMC, where all the shell proteins were found to be oriented with the concave side facing out of the structure[23].

Overall, this work demonstrates a concept for performing and evaluating rational protein design in the cell, specifically, making hybrid scaffolds comprising *de novo*-designed peptides and natural proteins, which can be engineered on the micron scale within the *E. coli* cytoplasm. Visualization of filaments with and without appended ancillary proteins, and of those broadly distributed filaments or those localized to the inner membrane, demonstrates the potential of the system as a universal scaffold for the attachment, dispersion or localization of targeted cargo throughout the cell. We believe that these features and properties of the cytoscaffold, coupled with its ease of decoration and remodelling within cells, will enable applications in biotechnology and synthetic biology. More generally, this ability to design and engineer proteins in the cell could usher in a new era of rational protein design and engineering *in vivo*.

Acknowledgements

We are grateful to the Biotechnology and Biological Sciences Research Council of the UK for a strategic LoLa Award to MJW, DNW, PV and WFX (BB/M002969/1). DNW holds a Royal Society Wolfson Research Merit Award. We thank the Wolfson Bioimaging Facility and BrisSynBio, a BBSRC/EPSRC-funded Synthetic Biology Research Centre (L01386X), for access to confocal and electron microscopes; Kevin Howland for assistance with GC–MS analysis; Dr Richard Sessions and Ismail Uddin for preparing images used in Figure 1; Dr Leon Harrington and Prof. Dr Petra Schwille for advice on the MinD system; and the entire BMC-SAGE LoLa group for helpful discussions.

Author contributions

M.J.L made constructs, prepared samples for TEM and confocal analysis, imaged samples by TEM, purified nanotubes and analyzed them by TEM, AFM and conducted the ethanol production experiments and analyses. J.M. undertook tomography and 3D reconstructions. L.H. undertook CLEM sample preparation and imaging. D.A. undertook confocal imaging. I.R.B. sectioned samples for TEM analysis. W.F.X. assisted with AFM and statistical analysis. M.J.L., J.M., L.H., J.M.F., S.F., P.V., D.N.W. and M.J.W designed the experiments. All authors contributed to the manuscript.

Competing Financial Interests

The authors declare no competing financial interests.

Author Information

Reprints and permissions information is available at www.nature.com/reprints. Correspondence and requests for materials should be addressed to m.j.warren@kent.ac.uk or D.N.Woolfson@bristol.ac.uk

References:

1 Polka, J. K., Hays, S. G. & Silver, P. A. Building Spatial Synthetic Biology with Compartments, Scaffolds, and Communities. *Cold Spring Harb. Perspect. Biol.* **8**, pii: a024018 (2016).

2 Zhang, Y. *et al.* Using unnatural protein fusions to engineer resveratrol biosynthesis in yeast and Mammalian cells. *J. Am. Chem. Soc.* **128**, 13030-13031 (2006).

3 Grinkova, Y. V., Denisov, I. G. & Sligar, S. G. Engineering extended membrane scaffold proteins for self-assembly of soluble nanoscale lipid bilayers. *Protein Eng. Des. Sel.* **23**, 843-848 (2010).

4 Delebecque, C. J., Silver, P. A. & Lindner, A. B. Designing and using RNA scaffolds to assemble proteins in vivo. *Nat. Protoc.* **7**, 1797-1807 (2012).

5 Zalatan, J. G. *et al.* Engineering complex synthetic transcriptional programs with CRISPR RNA scaffolds. *Cell* **160**, 339-350 (2015).

6 Agapakis, C. M., Boyle, P. M. & Silver, P. A. Natural strategies for the spatial optimization of metabolism in synthetic biology. *Nat. Chem. Biol.* **8**, 527-535 (2012).

7 Dueber, J. E. *et al.* Synthetic protein scaffolds provide modular control over metabolic flux. *Nat. Biotechnol.* **27**, 753-759 (2009).

8 Poshyvailo, L., von Lieres, E. & Kondrat, S. Does metabolite channeling accelerate enzyme-catalyzed cascade reactions? *PLOS One* **12**, doi:ARTN e0172673 (2017).

9 Wheeldon, I. *et al.* Substrate channelling as an approach to cascade reactions. *Nat. Chem.* **8**, 299-309 (2016).

10 Chowdhury, C., Sinha, S., Chun, S., Yeates, T. O. & Bobik, T. A. Diverse bacterial microcompartment organelles. *Microbiol. Mol. Biol. Rev.* **78**, 438-468 (2014).

11 Frank, S., Lawrence, A. D., Prentice, M. B. & Warren, M. J. Bacterial microcompartments moving into a synthetic biological world. *J. Biotechnol.* **163**, 273-279 (2013).

12 Kerfeld, C. A. & Erbilgin, O. Bacterial microcompartments and the modular construction of microbial metabolism. *Trends Microbiol* **23**, 22-34 (2015).

13 Cameron, J. C., Wilson, S. C., Bernstein, S. L. & Kerfeld, C. A. Biogenesis of a bacterial organelle: the carboxysome assembly pathway. *Cell* **155**, 1131-1140 (2013).

14 Kerfeld, C. A., Heinhorst, S. & Cannon, G. C. Bacterial microcompartments. *Annu. Rev. Microbiol.* **64**, 391-408 (2010).

15 Bobik, T. A., Havemann, G. D., Busch, R. J., Williams, D. S. & Aldrich, H. C. The propanediol utilization (pdu) operon of *Salmonella enterica* serovar Typhimurium LT2 includes genes necessary for formation of polyhedral organelles involved in coenzyme B12-dependent 1, 2-propanediol degradation.*J. Bacteriol.* **181**, 5967-5975 (1999).

16 Havemann, G. D. & Bobik, T. A. Protein content of polyhedral organelles involved in coenzyme B12-dependent degradation of 1,2-propanediol in *Salmonella enterica* serovar Typhimurium LT2. *J. Bacteriol.* **185**, 5086-5095 (2003).

17 Sampson, E. M. & Bobik, T. A. Microcompartments for B12-dependent 1,2-propanediol degradation provide protection from DNA and cellular damage by a reactive metabolic intermediate. *J. Bacteriol.* **190**, 2966-2971 (2008).

18 Fan, C. & Bobik, T. A. The N-terminal region of the medium subunit (PduD) packages adenosylcobalamin-dependent diol dehydratase (PduCDE) into the Pdu microcompartment. *J. Bacteriol.* **193**, 5623-5628 (2011).

19 Fan, C. *et al.* Short N-terminal sequences package proteins into bacterial microcompartments. *Proc. Natl. Acad. Sci. USA* **107**, 7509-7514 (2010).

20 Fan, C., Cheng, S., Sinha, S. & Bobik, T. A. Interactions between the termini of lumen enzymes and shell proteins mediate enzyme encapsulation into bacterial microcompartments. *Proc. Natl. Acad. Sci. USA* **109**, 14995-15000 (2012).

21 Lawrence, A. D. *et al.* Solution structure of a bacterial microcompartment targeting peptide and its application in the construction of an ethanol bioreactor. *ACS Synth. Biol.* **3**, 454-465 (2014).

22 Jakobson, C. M., Tullman-Ercek, D., Slininger, M. F. & Mangan, N. M. A systems-level model reveals that 1,2-Propanediol utilization microcompartments enhance pathway flux through intermediate sequestration. *PLOS Comput. Biol.* **13**, doi:ARTN e1005525 (2017).

23 Sutter, M., Greber, B., Aussignargues, C. & Kerfeld, C. A. Assembly principles and structure of a 6.5-MDa bacterial microcompartment shell. *Science* **356**, 1293-1297 (2017).

24 Cho, H. The role of cytoskeletal elements in shaping bacterial cells. *J. Microbiol. Biotechnol.* **25**, 307-316 (2015).

25 Cabeen, M. T. & Jacobs-Wagner, C. Bacterial cell shape. *Nat. Rev. Microbiol.* **3**, 601-610 (2005).

26 Cabeen, M. T. & Jacobs-Wagner, C. The bacterial cytoskeleton. *Annu. Rev. Genet.* **44**, 365-392 (2010).

27 Parsons, J. B. *et al.* Synthesis of empty bacterial microcompartments, directed organelle protein incorporation, and evidence of filament-associated organelle movement. *Mol. cell* **38**, 305-315 (2010).

28 Chowdhury, C. *et al.* Selective molecular transport through the protein shell of a bacterial microcompartment organelle. *Proc. Natl. Acad. Sci. USA* **112**, 2990-2995 (2015).

29 Crowley, C. S. *et al.* Structural insight into the mechanisms of transport across the *Salmonella enterica* Pdu microcompartment shell. *J. Biol. Chem.* **285**, 37838-37846 (2010).

30 Pang, A., Frank, S., Brown, I., Warren, M. J. & Pickersgill, R. W. Structural insights into higher order assembly and function of the bacterial microcompartment protein PduA. *J. Biol. Chem.* **289**, 22377-22384 (2014).

31 Thomas, F., Boyle, A. L., Burton, A. J. & Woolfson, D. N. A set of de novo designed parallel heterodimeric coiled coils with quantified dissociation constants in the micromolar to sub-nanomolar regime. *J. Am. Chem. Soc.* **135**, 5161-5166 (2013).

387 32 Lee, M. J., Brown, I. R., Juodeikis, R., Frank, S. & Warren, M. J. Employing bacterial
388 microcompartment technology to engineer a shell-free enzyme-aggregate for
389 enhanced 1,2-propanediol production in *Escherichia coli*. *Metab. Eng.* **36**, 48-56
390 (2016).
391 33 Fletcher, J. M. *et al.* Self-assembling cages from coiled-coil peptide modules.
392 *Science* **340**, 595-599 (2013).
393 34 Weber, B. *et al.* Automated tracing of microtubules in electron tomograms of plastic
394 embedded samples of *Caenorhabditis elegans* embryos. *J. Struct. Biol.* **178**, 129-138
395 (2012).
396 35 Johnson, E. *et al.* Correlative in-resin super-resolution and electron microscopy using
397 standard fluorescent proteins. *Sci Rep* **5**, 9583 (2015).
398 36 Mueller-Reichert, T. & Verkade, P. *Correlative Light and Electron Microscopy II;*
399 *Methods in Cell Biology* Vol. 124 (Academic Press, 2014).
400 37 Szeto, T. H., Rowland, S. L., Habrukowich, C. L. & King, G. F. The MinD membrane
401 targeting sequence is a transplantable lipid-binding helix. *J. Biol. Chem.* **278**, 40050-
402 40056 (2003).
403 38 Noël C. R., Cai F., & Kerfeld C. A. Purification and Characterization of Protein
404 Nanotubes Assembled from a Single Bacterial Microcompartment Shell Subunit. *Adv.*
405 *Mater. Interfaces* **3**, 1500295 (2015).
406 39 Lewicka, A. J. *et al.* Fusion of pyruvate decarboxylase and alcohol dehydrogenase
407 increases ethanol production in *Escherichia coli*. *ACS Synth. Biol.* **3**, 976-978 (2014).
408
409
410
411 **Figure Legends**
412
413 **Figure 1. Transmission electron micrographs and analysis of PduA*-based constructs**
414 **and filaments in *E. coli*.** (**a**) Untagged PduA* filaments. (**b**,**c**) CC-Di-A–PduA* (**b**) and CC-

Di-B–PduA* (**c**) filaments. Scale bars in **a**–**c**, 200 nm. (**d**) Histogram showing the diameter of CC-Di-B-PduA* filaments (n = 100). (**e**) Histogram showing lengths of CC-Di-B-PduA* filaments based on a 250 nm tomogram rendering shown in **f** (n = 739). (**f**) 3D render of CC-Di-B–PduA* filaments in *E. coli* based on a 250 nm tomogram. Scale bar in **f**, 500 nm. See also **Supplementary Video 1**.

Figure 2. Localization of fluorescent proteins to a bacterial cytoscaffold. (**a**) Co-expression of CC-Di-B–PduA* with CC-Di-A–Citrine, indicated by Citrine fluorescence. (**b**–**e**) Correlative Light Microscopy of a strain expressing CC-Di-B–PduA* and CC-Di-A–GFP, encompassing TEM (**b**), GFP fluorescence (**c**), overlay (**d**), and detail of the overlaid image (**e**). (**f**–**h**) Fluorescence of cells expressing CC-Di-B–PduA*, CC-Di-A–Citrine, and CC-Di-A–mCherry, including Citrine signal (**f**), mCherry signal (**g**), and overlay of the two (**h**). Scale bars in **a**,**f**–**h**, 5 μm; scale bars in **b**–**e**, 500 nm.

Figure 3. Ethanol production *in vivo*. Graph showing ethanol content of the growth medium over time normalized to an OD_{600} = 1. Open circles, *E. coli* strain transformed with empty plasmids (pET14b and pLysS); closed circles, strain producing CC-Di-B–PduA* only; open triangles, strain producing CC-Di-A–Pdc and CC-Di-A–Adh; closed triangles, strain producing CC-Di-A–Pdc, CC-Di-A–Adh and CC-Di-B–PduA*. Data points represent an average of three independent experiments; error bars, s.d.

Figure 4. Targeting the bacterial cytoscaffold to the inner membrane of *E. coli*. (**a**) Box-and-whisker plots showing the number of filaments associated with the inner membrane for 3 strains expressing variants of the CC-Di-A/B–PduA* system. Plot 1 = CC-Di-B-PduA*, Plot 2 = CC-Di-B–PduA* + CC-Di-A–Citrine–MinD, Plot 3 = CC-Di-B–PduA* + CC-Di-C–Citrine–MinD. Boxes show first and third quartiles, solid line shows median, dotted lines give the mean and whiskers the minimum and maximum; 250 cells were analyzed for each of the 3 strains. Statistically significant differences (p=0.01) are indicated by **. (**b**) Confocal image of strain expressing CC-Di-A–Citrine–MinD. Scale bar, 5 μm. (**c**) TEM micrograph of strains producing CC-Di-B–PduA* plus CC-Di-A–Citrine–MinD. Arrows indicate transverse filaments. (**d**) Zoom in of area 1 in **c**. Scale bars in **c** and **d**, 200 nm.

Online Methods:

Cloning of coiled-coil fused constructs. DNA encoding CC-Di-A and CC-Di-B embedded within a GS linker followed by a hexahistidine tag and a thrombin cleavage sequence was synthesized and cloned into the *Xba*I/ *Nde*I sites of pET14b. A control sequence containing only a GS linker, hexahistidine tag and thrombin cleavage sequence was also synthesized and cloned by the same strategy. Synthesized DNA sequences and amino acid sequences are shown in Supplementary Table 2.

Expression of coiled coil constructs. *E. coli* BL21 * (DE3) competent cells were transformed with a plasmid (s) containing the gene(s) of interest, and plated onto LB agar plates supplemented with appropriate antibiotics (ampicillin 100 mg/L and/ or chloramphenicol 34 mg/L). For TEM analysis 50 mL of LB was inoculated 1:100 from an overnight starter culture and grown at 37 °C with shaking to an OD_{600} of ~ 0.4, protein production was induced by the addition of IPTG to a final concentration of 400 μM, cultures were subsequently incubated overnight at 19 °C with shaking. For time course analysis 500 mL of LB was inoculated, grown and induced as described previously. At time intervals 50 mL of media was removed for TEM analysis. For purification of nanotubes 250 mL LB was inoculated 1:100 from an overnight starter culture and grown 37 °C to an OD_{600} ~ 0.4. Protein production was induced by addition of IPTG to a final concentration of 400 μM, cultures were then incubated with shaking at 19 °C overnight. For confocal imaging experiments 50 mL of LB was inoculated 1:100 from an overnight starter culture and grown with shaking at 37 °C to an OD_{600} ~ 0.4. protein production was induced by addition of IPTG to a final concentration of 400 μM, cultures were then incubated with shaking at 19 °C for 4 hours.

***In vivo* ethanol production.** For in-vivo ethanol production, 100 mL of LB supplemented with 4% glucose and appropriate antibiotics was inoculated from overnight starter cultures to a starting OD_{600} of 0.05; cultures were grown at 28 °C for 120 hours with shaking at 150 rpm.

Protein production was induced by addition of IPTG to a final concentration of 400 μM after 4 hours of growth. During growth, 1 mL samples were removed at 0, 2, 4, 6, 12, 24, 48, 72, 96 and 120 hours for GC/MS analysis of the growth medium. Samples (1 mL) were also taken at each time point for SDS-PAGE analysis. Additional samples (5 mL) were taken after 24 hours for TEM analysis.

Western blot analysis. Nitrocellulose membranes following transfer and blocking were incubated in primary antibody (rabbit anti-PduA 1 μg/ mL or mouse anti-His (Sigma Aldrich) 1:3000) followed by incubation in a secondary antibody coupled to alkaline phosphatase (Goat Anti-Rabbit IgG (H+L) Alkaline Phosphatase Conjugate (Bio-Rad) 1:3000 or Anti-Mouse IgG (H+L), AP Conjugate (Promega) 1:5000). Bands were visualized by incubation in substrate 5-bromo-4-chloro-3-indolyl phosphate/nitro blue tetrazolium (BCIP/NBT).

TEM analysis of cells. Cells grown as described previously were harvested by centrifugation at 3000 x g for 10 minutes. The cell pellet was resuspended in 2 mL 2.5% (w/v) glutaraldehyde in 100 mM sodium cacodylate buffer pH 7.2 (CAB) and fixed for 2 hours with gentle rotating (20 rpm). Cells were pelleted by centrifugation at 6000 x g for 2 minutes and were washed twice for 10 minutes with 100 mM CAB. Cells were post-fixed with 1% (w/v) osmium tetroxide in 100 mM CAB for 2 hours and subsequently washed twice with ddH_2O. Cells were dehydrated by incubation in an ethanol gradient, 50% EtOH for 10 minutes, 70% EtOH overnight, 90% EtOH for 10 minutes followed by three 10 minute washes in 100% dry EtOH. Cells were then washed twice with propylene oxide for 15 minutes. Cell pellets were embedded by resuspension in 1 mL of a 1:1 mix of propylene oxide and Agar LV Resin and incubated for 30 minutes with rotation. Cell pellets were infiltrated twice in 100% Agar LV resin. The cell pellet was re-suspended in fresh resin and transferred to a 1 mL Beem embedding capsule, centrifuged for 5 minutes at 3000 x g to concentrate the cells to the tip of the mould and incubated for 20 hours at 60 °C to polymerize.

499 Samples were ultra-thin sectioned on a RMC MT-XL ultra-microtome with a diamond knife
500 (diatome 45°). Sections (60 – 70 nm) were collected on un-coated 300 mesh copper grids.
501 Grids were stained by incubation in 4.5% (w/v) uranyl acetate in 1% (v/v) acetic acid solution
502 for 45 minutes followed by washing in a stream of ddH_2O. Grids were then stained with
503 Reynolds lead citrate for 7 minutes followed by washing in a stream of ddH_2O. Electron
504 microscopy was performed using a JEOL-1230 transmission electron microscope equipped
505 with a Gatan multiscan digital camera operated at an accelerating voltage of 80 kV

506 **Tomography.** Sections (250 nm) were cut from the existing blocks and 15nm gold fiducials
507 (Aurion, TomoSol solution) were applied to both surfaces of the sections. The sections were
508 imaged at 200 kV in a Tecnai 20 TEM (FEI, the Netherlands) and double tilt series images
509 acquired between -62° to +69.5° (first axis) and -68° to +69.5° (second axis) with 1.5°
510 (above 50°) and 2° increments (below 50°). The pixel size on the 4k by 4k FEI Eagle camera
511 was 0.74nm. The resulting tomograms were reconstructed and combined using IMOD
512 software[40,41]. The tube-like structures were modelled automatically using the AMIRA
513 XTracing Extension of the AMIRA software suite, developed for automatic tracing of
514 microtubules[34]. A cylinder template is correlated with the data to find and search for the
515 centre lines of tubes. A small cropped area was used to refine the fitting parameters as
516 shown in Supplementary Movie S2 and these were then applied to the full data set. AMIRA
517 software was further used for visualizing the data.

518 **Measurements of *in vivo* nanotubes.** Diameter measurements of 100 nanotubes from 10
519 cells were calculated in ImageJ[42]. Length measurements were calculated automatically
520 using the XTracing extension of the AMIRA software suite. Cropping box measurements
521 were removed manually from the dataset, leaving a total of 739 tubes.

522 **Purification of CC-Di-B-PduA*.** CC-Di-B tagged PduA* was overproduced as described
523 previously. Cells were harvested by centrifugation at 2683 x g. A 1 g wet cell pellet was
524 resuspended in 20 mL Yeast Protein Extraction Reagent (Thermo Scientific) supplemented

with Protease Inhibitor Cocktail Tablets, EDTA-Free (Sigma-Aldrich) and 500 Units Benzonase® Nuclease (Merck) and incubated for 3 hours at room temperature with gentle shaking. CC-Di-B-PduA* nanotubes were pelleted from the lysate by centrifugation for 5 minutes at 11,300 x g, the pellet was resuspended in 2 mL of 20 mM Tris-HCl, pH 8, containing 20 mM NaCl. The suspension was centrifuged for 5 minutes at 11,000 x g, the resulting nanotube containing pellet was resuspended in 20 mM Tris-HCl, pH 8, and centrifuged again as above. The supernatant was removed and adjusted with a solution of 5M NaCl to give a final concentration of 80 mM. A final centrifugation step as above was performed and the resulting pellet was analyzed for the presence of PduA* nanotubes.

Analysis of purified nanotubes. TEM: Following purification, 20 µL of CC-Di-B-PduA* nanotubes were deposited onto formvar, carbon coated 300 mesh copper grids and incubated to 5 minutes. Glutaraldehyde (20 µL of 2.5 % (v/v)) in PBS was then added and incubated for a further 5 minutes before washing in 3 drops of 2.5 % (v/v) glutaraldehyde in PBS followed by 3 drops of ddH_2O. Grids were stained with 2% (w/v) aqueous uranyl acetate and subsequently dried. Electron microscopy was performed using a JEOL-1230 transmission electron microscope equipped with a Gatan multiscan digital camera operated at an accelerating voltage of 80 kV.

AFM: Purified CC-Di-B-PduA* nanotubes (20 µL) nanotubes were deposited onto freshly cleaved mica surfaces and incubated for 5 minutes followed by the addition of 20 µL 2.5 % (v/v) glutaraldehyde in PBS. Surfaces were washed 3 times with 1 mL of ddH_2O then dried under a gentle stream of N_2. Images were acquired in air at 20 °C using a Bruker MultiMode 8 Scaning probe microscope operating under Peak-Force tapping mode (ScanAsyst, Bruker) with a ScanSsyst-air probe (Bruker). Areas (10 µm x 10 µm) were scanned at a resolution of 4096 x 4096 pixels. Bow and tilt were removed using NanoScope Analysis 1.4 (Bruker).

Confocal imaging. Following growth and induction of protein expression 1 mL of cells was harvested by centrifugation at 3000 x g. The resulting cell pellet was washed 3 times in PBS

551 before incubation for 15 minutes in 2% (w/v) formaldehyde in PBS, cells were then washed a
552 further 3 times in PBS. Cells (10 µL) were pipetted onto a 1.5 thickness coverslip before
553 being inverted onto a drop of ProLong Gold antifade mountant (Life Technologies) on a
554 glass slide Slides were incubated at room temperature in the dark for 24 hours to cure.
555 Images were acquired on a Leica TCS SP8 system attached to a Leica DMi8 inverted
556 microscope (Leica Microsystems). Excitation light (514 nm for mCitrine or 594 nm for
557 mCherry) was provided by a white light laser with a repetition rate of 80 MHz. Images were
558 acquired using a 100 x 1.4 NA oil immersion objective and fluorescence was detected
559 through bandpasses of 520 – 570 nm (mCitrine detection) or 600 - 650 nm (mCherry
560 detection).

561 **Correlative Light Electron Microscopy.** Cells were harvested by centrifugation at 3000 x g
562 for 5 minutes. Cells (1µL) were loaded into a 0.1 mm membrane carrier (Leica) and vitrified
563 by high pressure freezing (EMPACT2 + RTS, Leica). Frozen membrane carriers were
564 transferred into 1 mL of freeze substitution medium (0.2% uranyl acetate, 5% H_2O, in
565 acetone) and held at -90°C for 5 hours in an automated freeze substitution unit (AFS2,
566 Leica) equipped with an attachment for automated reagent exchange (Freeze Substitution
567 Processor, FSP, Leica) (*30*). Samples were warmed to -45°C at a rate of 5 °C/hour, held at -
568 45°C for 2 hours before washes in acetone and ethanol for 30 minutes each. Samples were
569 then infiltrated with 25, 50 and 75% dilutions of Lowicryl HM20 resin for 3 hours each before
570 infiltrating with 100% resin overnight, followed by a further 3 changes of resin for 2 hours
571 each. UV polymerization was performed over approximately 48 hours; initially at -45°C for 16
572 hours, before warming to 0°C at a slope of 5°C/hour and finally at 0°C for approximately 14
573 hours.

574 Following polymerization, blocks were removed from flow through containers and carriers
575 were detached using liquid nitrogen and the specimen carrier detaching tool (Leica) heated
576 to 40°C. Blocks were trimmed and sectioned with a 45° diamond knife using an EM UC6
577 microtome (Leica). 70 and 300 nm thick sections were collected on carbon-coated pioloform

films on H6 copper finder grids (Agar Scientific). Grids were air dried, mounted in PBS between a glass slide and coverslip and imaged by light microscopy using a Leica DMI4000 B inverted epifluorescence microscope fitted with a 63x oil immersion lens (NA 1.4). After imaging, the grids were washed in H_2O and air dried before imaging in TEM. Image registration of light and electron microscopy images was performed using the eC-CLEM plugin in ICY[43].

Analysis of enzyme levels. Relative amounts of Pdc and Adh were quantified by western blot. Total cell lysate samples, adjusted to cell number were analyzed by SDS-PAGE and subsequently western blot analysis. Peak areas were quantified using the gel analysis tool in Image J. Due to the higher molecular weight band close to CC-Di-A-Adh half of this peak was quantified on the assumption that the peak was symmetrical. Measurements were repeated for each of the cultures.

MinD colocalization . DNA encoding the c-terminal membrane-associating region of MinD was synthesized and cloned into the *Spe*I/*Blp*I sites of pET_CC_Di_A_Citrine_No_Stop and pET_C_Citrine_No_Stop. Cells were transformed as described previously and grown in LB media at 37 °C with shaking to an OD_{600} ~ 0.4, protein production was induced by addition of IPTG to a final concentration of 400 µM. Cultures were then incubated with shaking at 19 °C for 4 hours. Cells were harvested, fixed, embedded and sectioned as described previously. A total of 250 cells in the transverse orientation for each strain were analyzed for the presence and location of transverse CC-Di-B-PduA* nanotubes. Statistical analysis was performed in Minitab Software version 17 using a one-way ANOVA (Analysis of Variance) at the 99% level with posthoc analysis by Tukey's test.

Data Availability Statement

All data generated or analyzed during this study are included in this published article (and supplementary information files) or are available from the corresponding authors on reasonable request.

Methods References

40 Kremer, J. R., Mastronarde, D. N. & McIntosh, J. R. Computer visualization of three-dimensional image data using IMOD. *J. Struct. Biol.* **116**, 71-76 (1996).

41 Mastronarde, D. N. Dual-axis tomography: An approach with alignment methods that preserve resolution. *J. Struct. Biol.* **120**, 343-352 (1997).

42 Schindelin, J. *et al.* Fiji: an open-source platform for biological-image analysis. *Nat. Methods* **9**, 676-682 (2012).

43 Paul-Gilloteaux, P. *et al.* eC-CLEM: flexible multidimensional registration software for correlative microscopies. *Nat. Methods* **14**, 102-103 (2017).

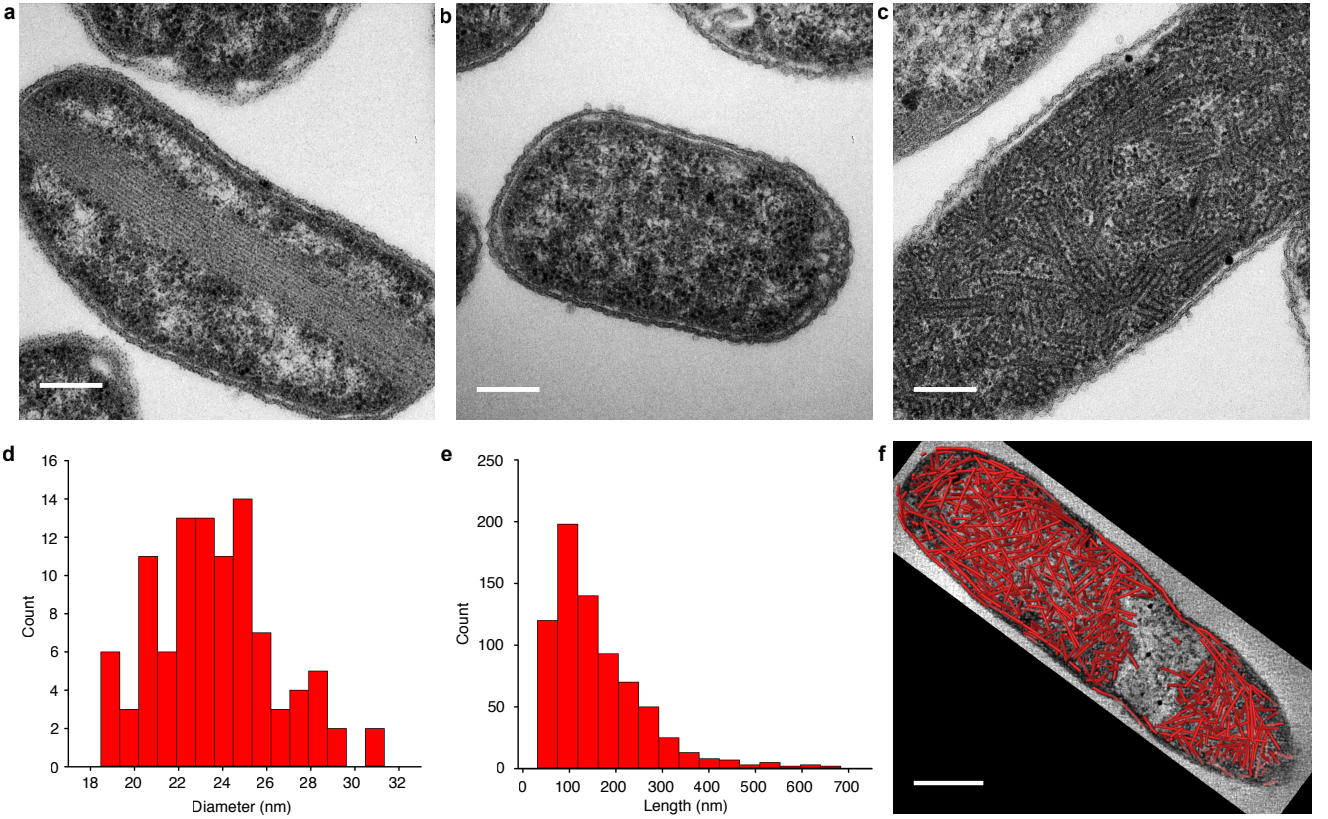
a
b
c
d
Count
Diameter (nm)
e
Count
Length (nm)
f

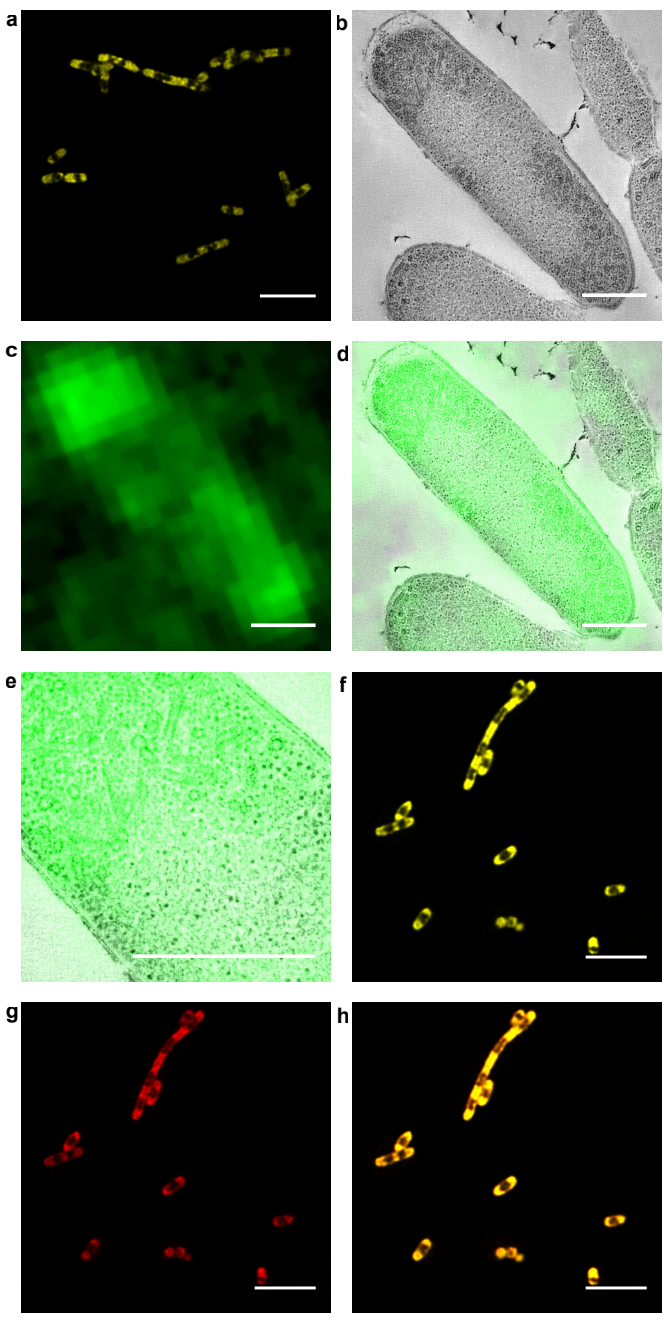
a
b
c
d
e
f
g
h

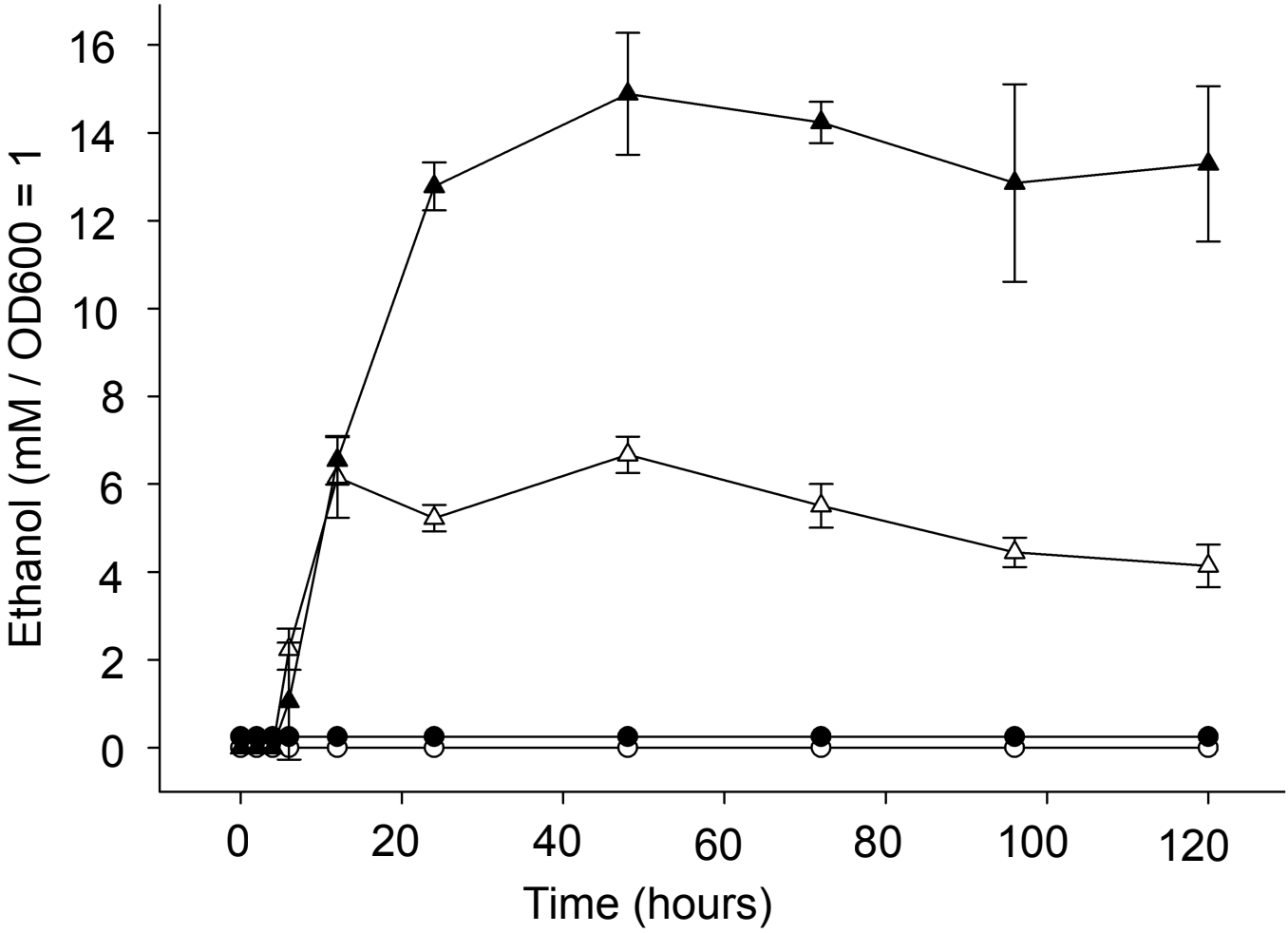
Ethanol (mM / OD600 = 1
16
14
12
10
8
6
4
2
0
0
20
40
60
80
100
120
Time (hours)

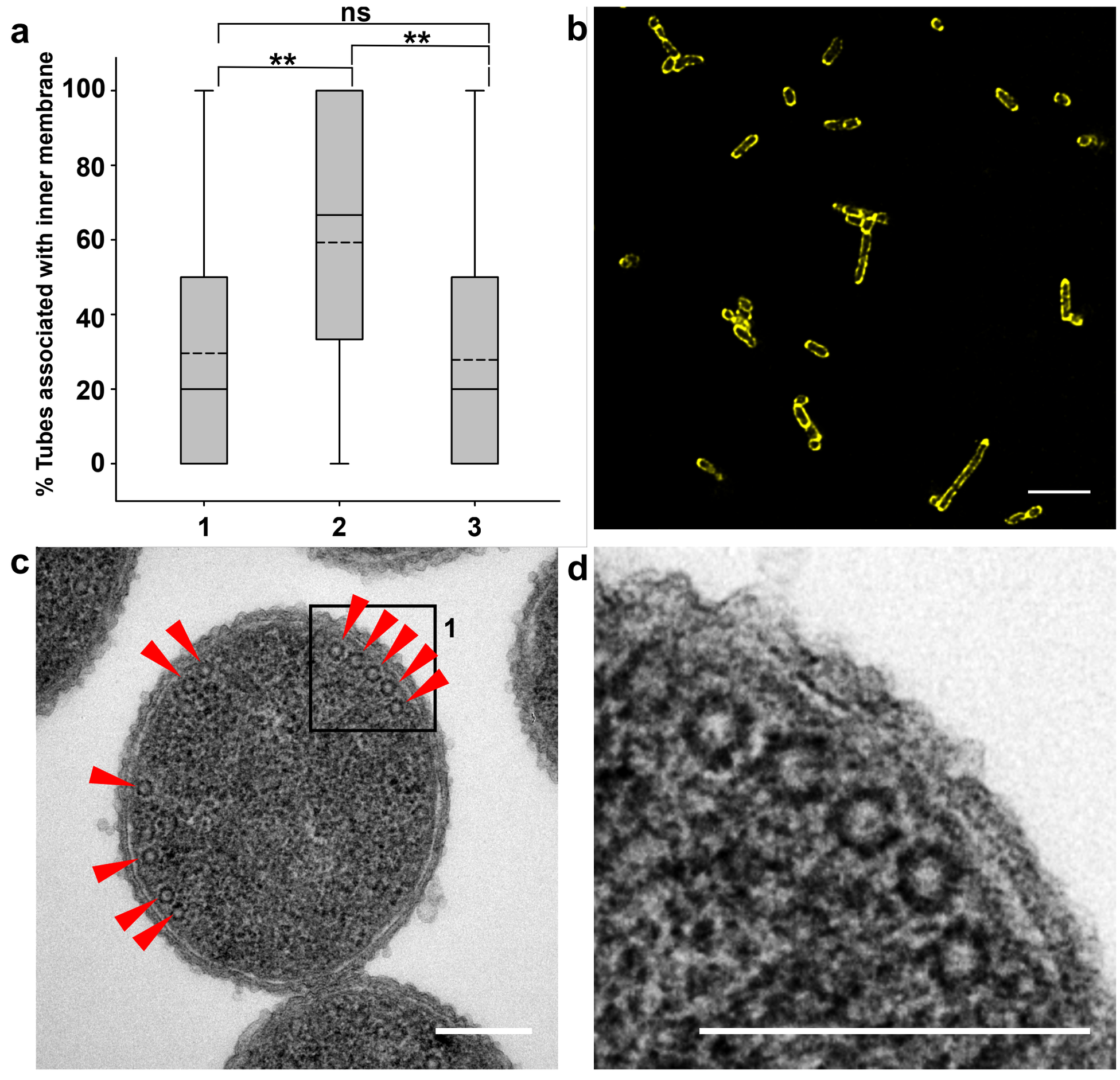
a
ns
**
**
% Tubes associated with inner membrane
100
80
60
40
20
0
1
2
3
b
c
1
d